Progress In Electromagnetics Research C, Vol. 87, 97–106, 2018

Reflective Metasurface for Vortex Wave Generating and Divergence Reducing in X-Band

Xiaohang Dong, Hengyi Sun, Changqing Gu*, Zhuo Li, Xinlei Chen, and Baijie Xu

Abstract—In this paper, a novel and simple solution for generating vortex electromagnetic wave and reducing divergence simultaneously in a wideband is presented. Based on phase gradient metasurface, we design a metasurface that can convert an ordinary electromagnetic wave into a vortex one and focus the vortex wave in X-band. Double layer rectangular metal patch units of different sizes are arranged in a certain order to compose the metasurface. The phase introduced by the metasurface is superimposed by the vortex phase and focusing phase. Compared to a general vortex wave metasurface, the simulation results show that the divergence of the reflected vortex wave generated by our designed metasurface is dramatically reduced in the frequency range from 8 GHz to 12 GHz. It is indicated that the designed metasurface has a highly efficient focusing effect, and it is also in a good agreement with the theoretical analysis. The proposed reflective metasurface paves an effective way to reduce the divergence of vortex electromagnetic wave for OAM-based system in microwave and radio frequency.

1. INTRODUCTION

The angular momentum contains a spin angular momentum (SAM) in relation to the polarization [1] and an orbital angular momentum (OAM) associated with the spatial distribution [2]. Although the OAM has long been recognized, it was not until 1992 that Allen et al. demonstrated light beams with an azimuthal phase dependence of $e^{-jl\varphi}$ possessing an OAM [3]. Theoretically, the topological charge of OAM can be any integer value, and it will be many times greater than the SAM. As the orthogonality between different topological charges contributes to distinguish an electromagnetic wave with the same frequency by OAM, the information can be modulated by the helical wave-front, which can boost communication capacity [4, 5]. Vortex waves carrying OAM, characterized by having a helical wave-fronts and an intensity null running along the axis of the beam [6], have drawn great attention of worldwide academia. In the last few years, OAM applied to optics has been explosively developed [4–9], while the researches of OAM in the radio frequency region move slowly for a long time. Until 2007, Thide et al. applied the theory of OAM to low frequency region and proved that vortex wave can be generated by circular antenna array [10]. Thus, the application of OAM in the microwave and radio domains is growing more and more popular. In 2010, Mohammadi et al. studied the vortex waves generated by a circular antenna array theoretically [11]. And later, Tamburini et al. confirmed that the wireless communication via vortex waves could become a reality by experiment [12].

Over the years, there are many progressive explorations on the application of vortex wave in multidisciplinary field such as communications [12], detection [13] and imaging [14] for its obvious advantages. The generation of vortex wave is the basis for the application of vortex wave. Therefore, how to generate vortex wave effectively becomes one of the most important aspects of OAM-based system. Thus far, the vortex wave can be generated by antenna arrays [10], spiral phase plate [11], helicoidal

Received 5 July 2018, Accepted 31 August 2018, Scheduled 25 September 2018

* Corresponding author: Chang Qing Gu (gucq@nuaa.edu.cn).

The authors are with the Key Laboratory of Radar Imaging and Microwave Photonics, Ministry of Education, College of Electronic and Information Engineering, Nanjing University of Aeronautics and Astronautics, Nanjing 211106, China.

parabolic antenna [15], circular traveling-wave antenna [16], and metasurfaces [17–24]. Metasurface was used to generate vortex wave because of its ability to manipulate electromagnetic wave flexibly and the advantage of its thin structure [25]. Although fruitful progress has been achieved toward OAM across both optical and radio frequency domains, vortex wave generation is mostly limited to a narrow frequency band, and the angle of wave divergence is big that calls for immediate solution.

Due to the divergence characteristics of vortex wave, the center dark nucleus with zero intensity becomes larger and larger with the increase of the propagation distance. This paper devotes to the vortex wave generation and the divergence problem of the vortex wave. Since metasurface can flexibly change the phase and wave-front of the electromagnetic wave, we designed a simple reflective metasurface that can generate a vortex wave and reduce the divergence of the vortex wave from 8 GHz to 12 GHz. In our case, we firstly designed a general vortex wave metasurface as a reference. The generated vortex wave is focused by adding a focusing phase distribution to the proposed vortex wave generating metasurface. The simulation results show that the proposed metasurface makes the vortex wave converge effectively, constituting an important result for OAM-based system.

2. METASURFACE DESIGNS

By using the generalized Snell's laws, the phase gradient metasurface provides a new way for the OAM generator design [26]. From the spiral phase structure of vortex electromagnetic wave, we can know that the basic principle of vortex electromagnetic wave generation is to construct this phase distribution on the cross section perpendicular to the direction of propagation. In order to generate a vortex wave in a wide frequency band, the gradient of phase along the interface should be insensitive to frequency, which means that the phase difference of separate elements should remain basically unchanged in the design frequency band.

In our case, Figure 1 shows the geometry details of the unit cell. Each unit cell consists of two substrates and three metal layers. The period length of the unit cell is $p = 11$ mm, and the thickness of the metal is $t = 0.017$ mm; the length of the metal on the top is $a_1 = 0.8 \cdot a_2$. The substrate layers are F4B ($\varepsilon_r = 2.65$), and the substrate thickness is set to $d = 1.5$ mm.

By changing the length of the metal layer a_2 in the middle of the unit structure, the phase varies in the frequency range from 8 GHz to 12 GHz. It can be seen from Figure 2 that the reflection phase covers $0 - to - 2\pi$. The simulation results show that the reflection phase of the designed unit cell changes slowly at different frequencies and has good parallelism, which satisfies the requirement of phase difference coverage $0 - to - 2\pi$ and is beneficial to the realization of 8 GHz to 12 GHz wideband vortex wave metasurface designs. Based on the reflection phase characteristics of the single element, shown in Figure 2, we consider eight elements to cover the range. The concrete designed parameters and the corresponding reflection phases are shown in Table 1 as well.

The design of metasurface is divided into the design of a general vortex wave metasurface and the design of a metasurface to focus the generated vortex wave.

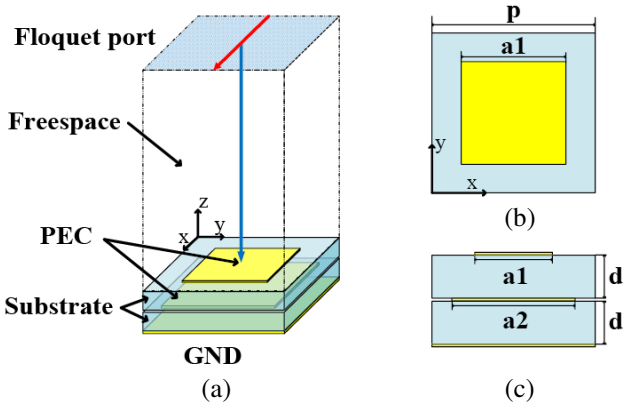

Figure 1. (a) Scheme of the unit cell used in the design. (b) and (c) are top view and front view of the unit cell respectively.

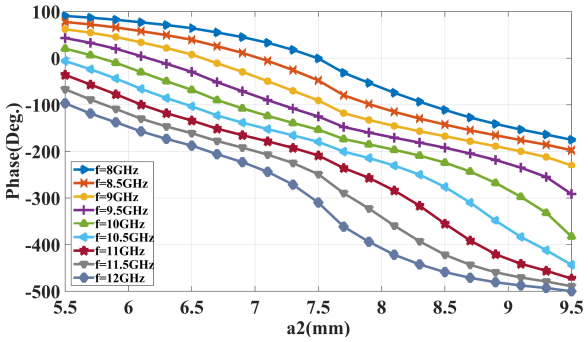

Figure 2. The phase of the reflection coefficient versus the length of a_2 from 8 GHz to 12 GHz.

Table 1. The size of the metallic patch layer and corresponding phase at 10 GHz.

N	Size of a_1 (mm)	Size of a_2 (mm)	Phase responses (degree)
1	4.64	5.80	0
2	5.00	6.25	-45
3	5.36	6.70	-90
4	5.80	7.25	-135
5	6.24	7.80	-180
6	6.80	8.50	-215
7	7.16	8.95	-270
8	7.36	9.20	-315

2.1. Metasurface for Generating Vortex Wave

To get vortex wave with an OAM mode number of l, a rotational phase factor $e^{-jl\varphi}$ related to the spatial azimuth should be added to the ordinary electromagnetic wave. If we consider a metasurface consists of $M \times N$ elements, a feeding antenna was taken as the excitation source at the position vector r_f impinging perpendicular incidence onto the structure, then, the phase shift required at each element for the OAM vortex wave at position $P(x_{mn}, y_{mn})$ can be obtained by:

$$\phi_{mn}^{C}(x_{mn}, y_{mn}) = \pm k_0 |\mathbf{r}_f - \mathbf{r}_{mn}| + k_0 \mathbf{r}_{mn} \cdot \hat{\mathbf{u}}_0 \pm l\varphi_{mn} \tag{1}$$

where k_0 is the wave vector, r_{mn} the position vector of the element, mn the position of column n in row m, and φ_{mn} the azimuthal angle of the mn element on the metasurface.

Based on the reflection phase characteristics of the single element illustrated in Figure 2, we consider these eight units (Table 1) to cover the $0 - to - 2\pi$ range. The compensation phase of each position $P(x_{mn}, y_{mn})$ is calculated according to Equation (1) and shown in Figure 4(a). The metasurface is designed to generate a vortex wave from 8 GHz to 12 GHz. As shown in Figure 4(b), the metasurface is a square array with the dimension of 330 mm $\times$ 330 mm, containing 30×30 elements with period size 11 mm $\times$ 11 mm. A Vivaldi antenna shown in Figure 3 is used as the feeding source in normal incidence. The distance between the Vivaldi antenna and the metasurface is 70 mm.

2.2. Metasurface for Focusing Vortex Wave

The vortex wave has a dark nucleus existing in the boresight direction, where the field intensity is zero, and the opening angle of the magnitude distribution along the propagation direction will get bigger as it propagates. To further reduce the divergence of the vortex wave, according to the principle of phase compensation, the phase distribution at the interface should satisfy the following Equation (2).

When the electromagnetic wave is incident vertically, the reflected wave will be focused according to the knowledge of geometric optics [27–31].

$$\phi_{mn}^{C}\left(x_{mn}, y_{mn}\right) = \pm k_0 \left|\mathbf{r}_f - \mathbf{r}_{mn}\right| + k_0 \mathbf{r}_{mn} \cdot \hat{\mathbf{u}}_0 \pm l\varphi_{mn} + k_0 \left(\sqrt{F^2 + x_{mn}^2 + y_{mn}^2} - F\right) \tag{2}$$

where F is the focus length.

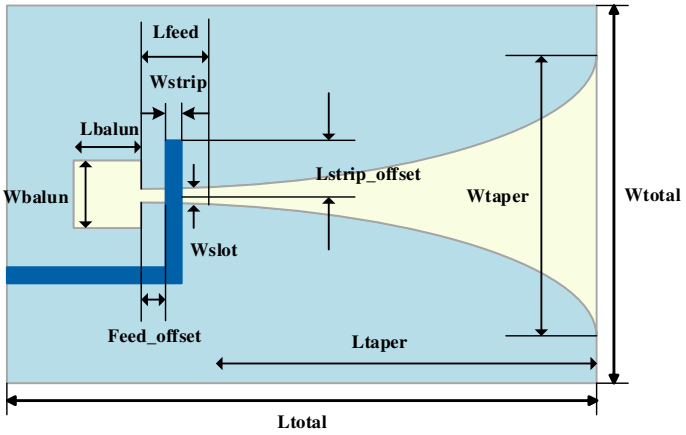

Figure 3. Scheme of the Vivaldi antenna. The length of the Vivaldi antenna is $Ltotal = 50.06\,\text{mm}$, while the width is $Wtotal = 37.5\,\text{mm}$; the taper length is $Ltaper = 37.5\,\text{mm}$, the taper width is $Wtaper = 18.75\,\text{mm}$; the balun length is $Lbalun = 5.06\,\text{mm}$, the balun width is $Wbalun = 5.06\,\text{mm}$; the slot width is $Wslot = 0.29\,\text{mm}$; the strip width is $Wstrip = 1.31\,\text{mm}$. And the thinckness of the substrate is set to $ts = 1.57\,\text{mm}$.

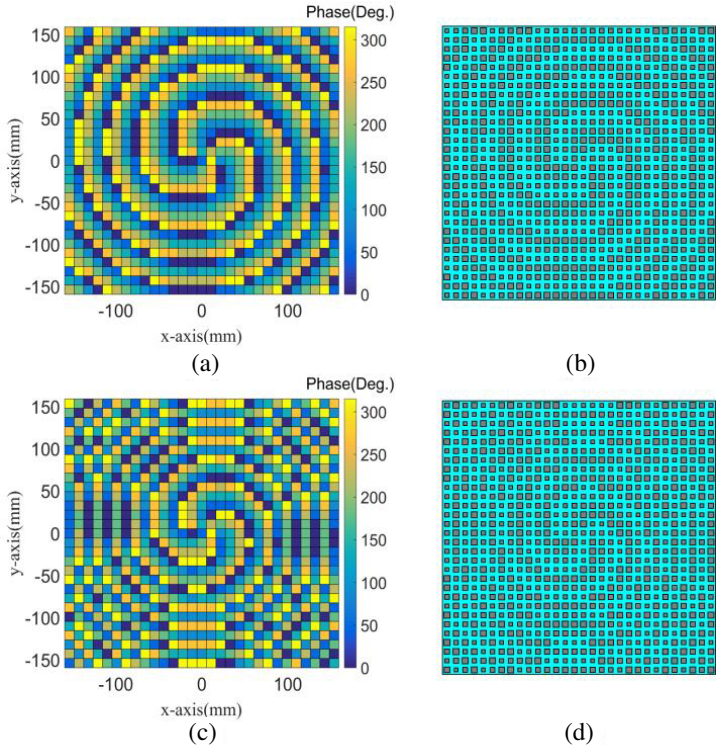

Figure 4. Reflection phase distribution on the metasurface required for (a) generated vortex wave with mode $l = 3$ and (c) generated focused vortex wave with mode $l = 3$. (b) (d) Scheme of the corresponding metasurface.

After the phase parameter is determined (Figure 4 (c)), the layouts of converging OAM-carrying metasurface can be readily achieved (Figure 4(d)) by conducting a geometrical mapping process.

3. SIMULATIONS AND ANALYSIS

The simulations were accomplished via the software CST Microwave Studio. The time domain solver is used for simulation, and the boundaries at the x, y and z directions are set as open (add space). The feeding antenna is located in front of the designed metasurface with 70 mm along the z-axis. On the one hand, the magnitude distribution (Figure 5 and Figure 8) and the phase distribution (Figure 6 and Figure 9) of the reflected wave indicate that, by impinging the feeding source on the reflective metasurface array, the wave-front of the reflected wave will be of helical form, and have a central singularity. It reveals that vortex wave is effectively generated by the proposed metasurface. On the other hand, when we consider combining focusing phase to reduce divergence, the reflected wave carrying spiral phase wave-front can be focused on certain point under the incidence. The simulation results of magnitude distribution for generating converged vortex wave are shown in Figure 8, and the corresponding phase distribution is shown in Figure 9. It can be observed clearly that the vortex wave converges as we proposed before.

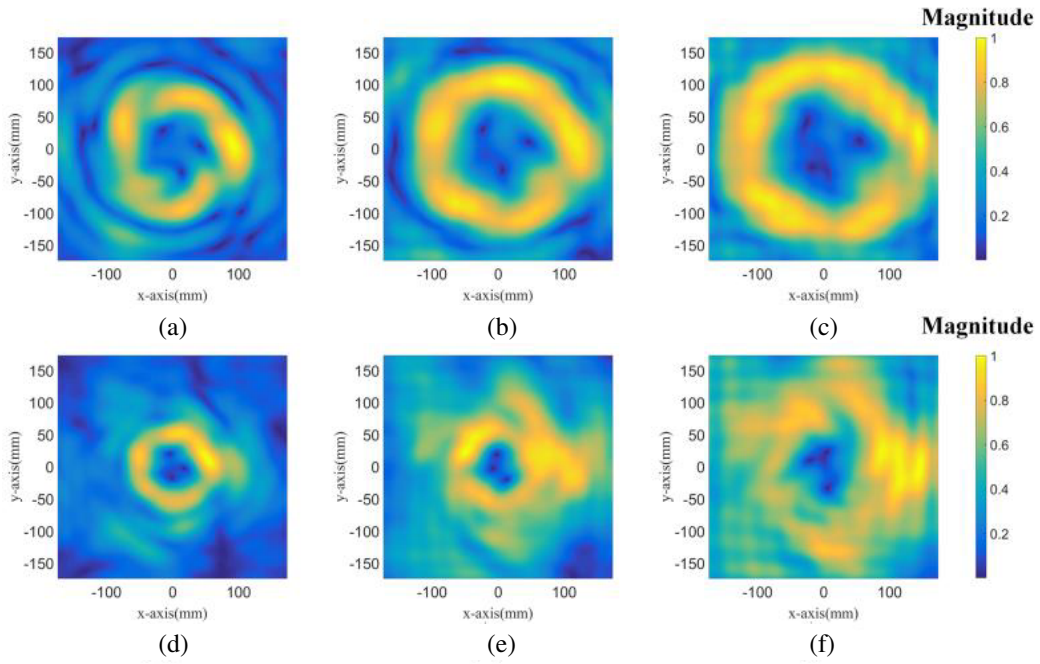

Figure 5. From left to right (a)–(c) are the normalized magnitude distribution of E-field on different observation planes at $z = 200$ mm, $z = 300$ mm, and $z = 400$ mm with mode $l = 3$ before adding the focusing phase at $f = 10$ GHz, and (d)–(f) are the distribution of E-field after adding the focusing phase at $f = 10$ GHz.

3.1. Converged Vortex Wave Generation

The distributions of E-field at $z = 200$ mm and $z = 300$ mm, and $z = 400$ mm are shown in Figures 5 and 6, respectively. The energy of each vortex wave would decrease according to propagation distance. Comparing the results at different distances, we can see that the helical form of the wave-front has not changed, and the generated vortex wave maintains a good stability as it propagates (Figure 6). In the meanwhile, the diameter of the ring-shape E-field intensity distribution generated by the converged vortex wave generator in Figures 5(d), (e), (f) is obviously smaller than that of the vortex wave generator

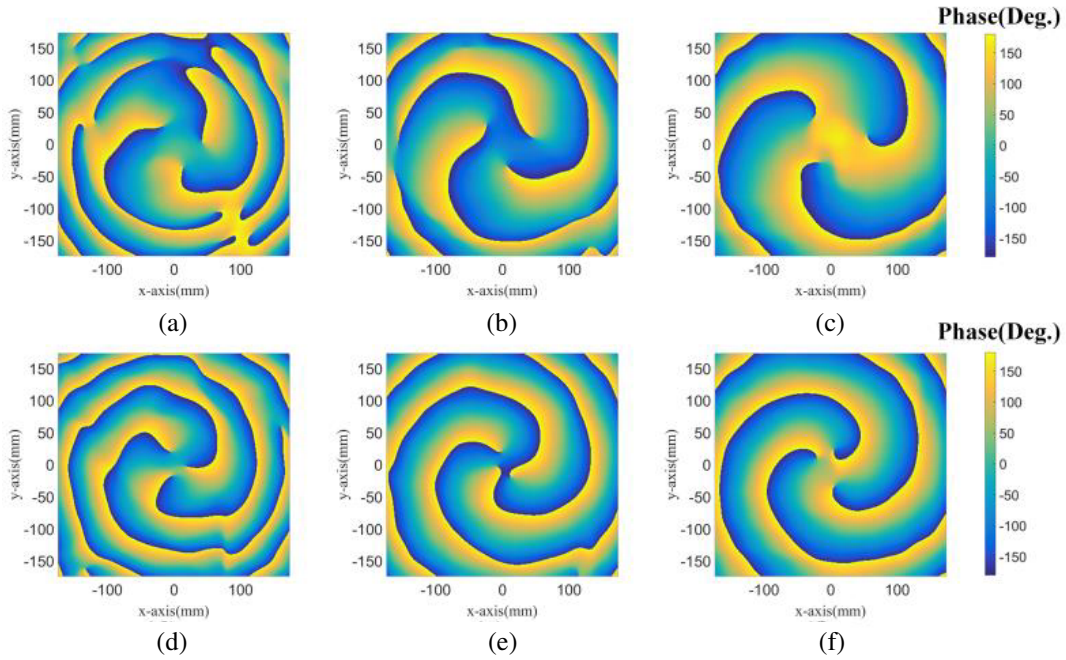

Figure 6. From left to right (a)–(c) are the corresponding phase distribution of E-field on different observation planes at $z = 200\,\text{mm}$, $z = 300\,\text{mm}$, and $z = 400\,\text{mm}$ with mode $l = 3$ before adding the focusing phase at $f = 10\,\text{GHz}$, and (d)–(f) are the distribution of E-field after adding the focusing phase at $f = 10\,\text{GHz}$.

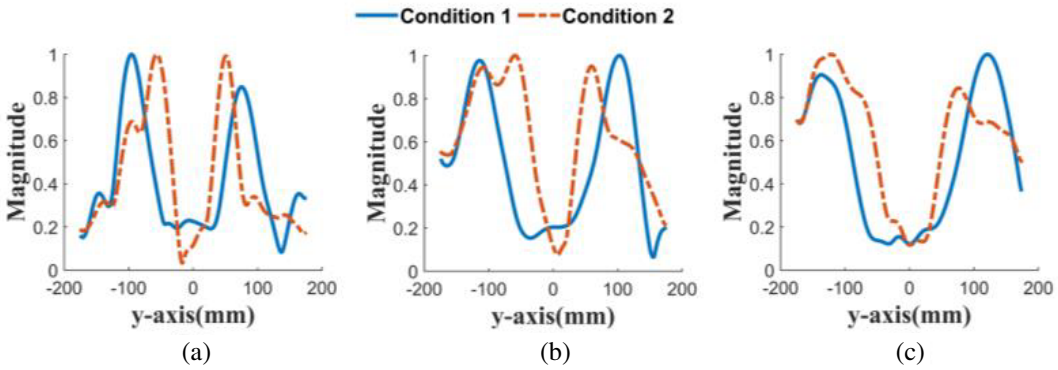

Figure 7. Normalized magnitude of the vortex wave on different observation plane (a) $z = 200\,\text{mm}$, (b) $z = 300\,\text{mm}$, and (c) $z = 400\,\text{mm}$ along the y-axis at the same frequency $f = 10\,\text{GHz}$. Condition 1 means the vortex wave generated by the no-focusing metasurface, while condition 2 means the vortex wave generated by the focusing metasurface.

in Figures 5(a), (b), (c). The simulation results for the normalized magnitude of the vortex wave generated by the designed metasurface along y-axis changing with propagating distance are shown in Figure 7. For the distances of $z = 200\,\text{mm}$, $z = 300\,\text{mm}$, and $z = 400\,\text{mm}$, the diameter of the central hole of the vortex wave generated by the focusing metasurface is 60% of that of the vortex wave generated by the no-focusing metasurface (Table 2). It illustrates that the metasurface for focusing vortex wave can concentrate the energy of the vortex beam into a smaller region, which is promising in OAM-based communication system.

Table 2. Diameter of the central hole on different observation plane at the same frequency $f = 10\,\text{GHz}$. $\lambda = 30\,\text{mm}$ is wavelength at $f = 10\,\text{GHz}$.

Observation plane	Before focusing	After focusing
$z = 200\,\text{mm}$	5.7λ	3.6λ
$z = 300\,\text{mm}$	7.2λ	4.2λ
$z = 400\,\text{mm}$	8.4λ	5.1λ

3.2. The Wideband Vortex Wave Behavior

To further illustrate the wideband converged vortex wave behavior, we presented E-field distribution results of the converged vortex metasurface from 8 GHz to 12 GHz in steps of 2 GHz. Similarly, the vortex wave with a central singularity in all cases and the phase distribution will be of helical form (Figure 9). The vortex wave of the same mode has different divergences at different frequencies, and the focus also has some deviation at different frequencies. Therefor, the reduction of divergence is also different at different frequencies. However, overall the consequences of different frequencies are consistent with that of 10 GHz (Figure 8). It can be seen that the diameter of the central hole is always about 55–65% of that of the vortex wave generated by the no-focusing metasurface (Figure 10). Specific values are shown in Table 3. By observing the phase wave-front variation at different frequencies, we can find that the operational bandwidth of the proposed reflective metasurface for vortex wave generating and focusing is from about 8 GHz to 12 GHz.

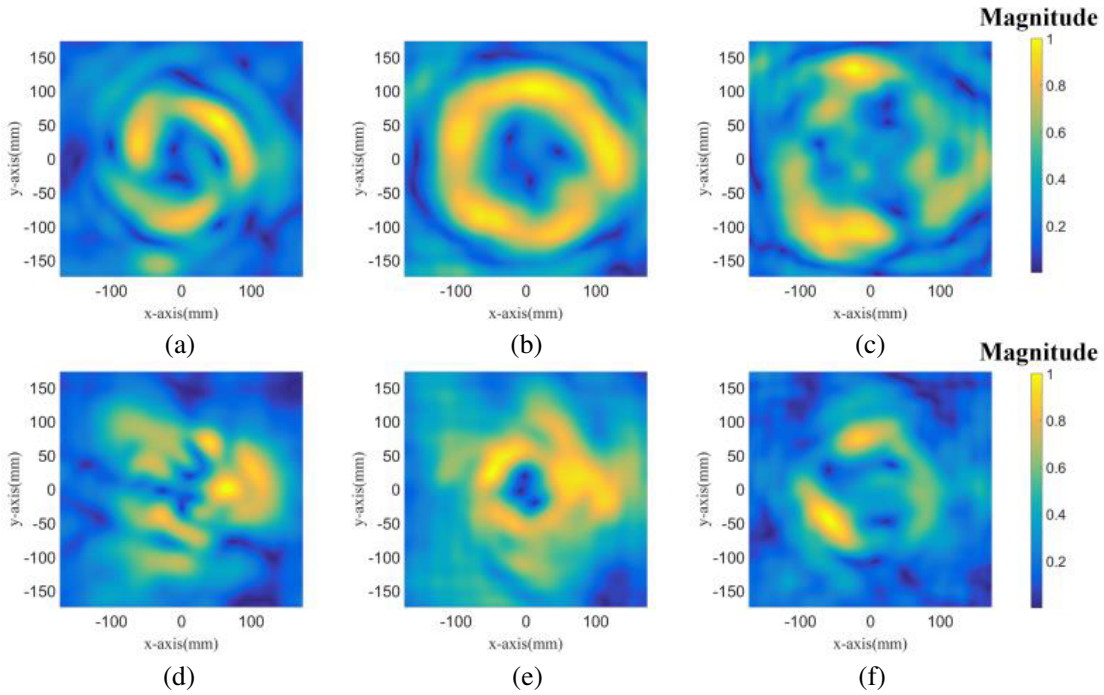

Figure 8. From left to right (a)–(c) are the normalized magnitude distribution of E-field on the observation plane at $z = 300\,\text{mm}$ with mode $l = 3$ at $f = 8\,\text{GHz}$, $f = 10\,\text{GHz}$, and $f = 12\,\text{GHz}$ before adding the focusing phase, and (d)–(f) are the distribution of E-field after adding the focusing phase.

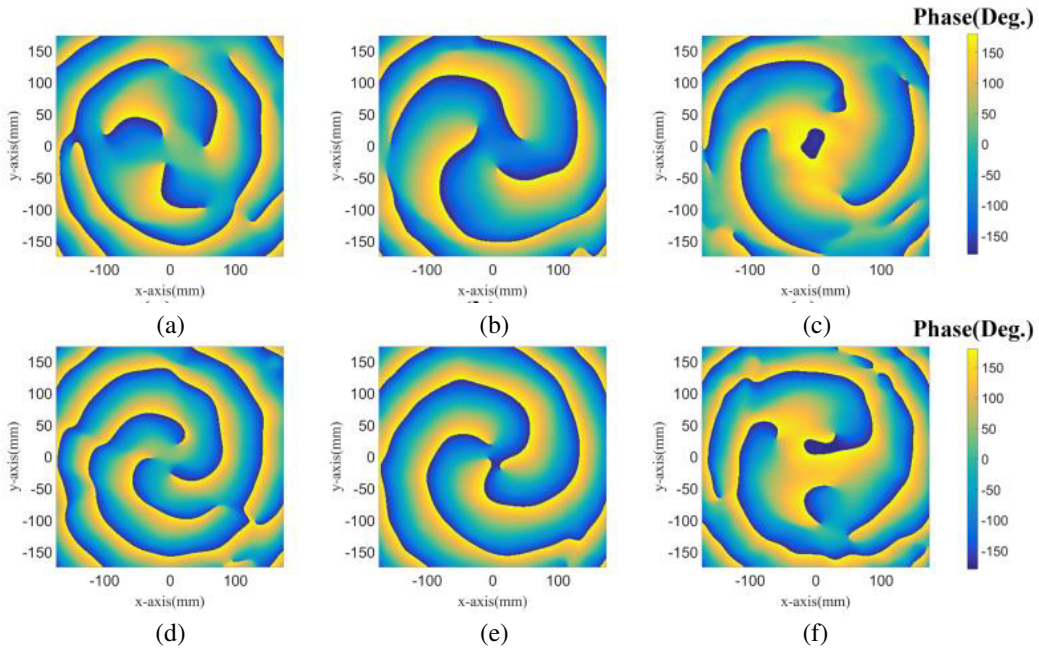

Figure 9. From left to right (a)–(c) are the corresponding phase distribution of E-field on the observation plane at $z = 300\,\text{mm}$ with mode $l = 3$ at $f = 8\,\text{GHz}$, $f = 10\,\text{GHz}$, and $f = 12\,\text{GHz}$ before adding the focusing phase, and (d)–(f) are the distribution of E-field after adding the focusing phase.

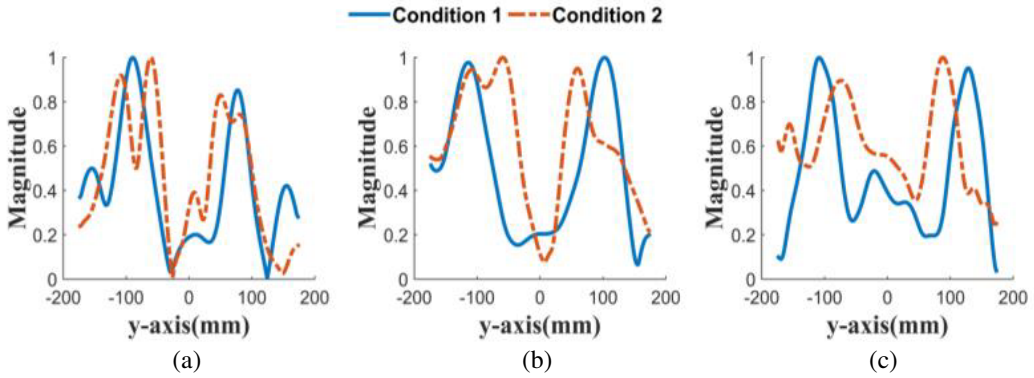

Figure 10. Normalized magnitude of the vortex wave on the same observation plane $z = 300\,\text{mm}$ along the axis $x = 0$ at (a) $f = 8\,\text{GHz}$, (b) $f = 10\,\text{GHz}$, and (c) $f = 12\,\text{GHz}$. Condition 1 means the vortex wave generated by the no-focusing metasurface, while condition 2 means the vortex wave generated by the focusing metasurface.

Table 3. Diameter of the central hole at different frequency on the same observation plane $z = 300\,\text{mm}$. $\lambda_1 = 37.5\,\text{mm}$, $\lambda_2 = 30\,\text{mm}$, $\lambda_3 = 25\,\text{mm}$ are wavelengths at 8 GHz, 10 GHz, and 12 GHz respectively.

Frequency	Before focusing	After focusing
$f = 8\,\text{GHz}$	$4.7\lambda_1$	$3.1\lambda_1$
$f = 10\,\text{GHz}$	$7.2\lambda_2$	$4.2\lambda_2$
$f = 12\,\text{GHz}$	$10.4\lambda_3$	$6.4\lambda_3$

4. CONCLUSION

A simple design of generating and focusing vortex wave with a metasurface in X-band is presented in this paper. Simulation demonstrated that vortex wave can be effectively generated with the metasurface in the wideband from 8 GHz to 12 GHz. Furthermore, by combining the spatial phase distribution of the vortex beam with that of a focusing phase, a converged vortex wave is obtained. Simulation results show that the diameter of a focused vortex wave is smaller than the regular vortex wave with the same topological charge. Compared to the traditional method of adding a parabolic reflector to the vortex wave generator, the complexity of the device is greatly reduced. We believe that our results provide an efficient alternative for generating vortex wave and reducing divergence simultaneously in the microwave region.

Since information can be encoded as OAM states, the proposed configuration may provide an effective way to generate vortex waves and less likely to suffer from divergence along the propagation path for OAM-based microwave wireless communication applications, which will greatly promote the study and application of vortex wave. With future improvement, we will explore the impact of focus setting and feeding source location on the effect of improving divergence. Subsequent experiments will be conducted to verify the relevant data.

ACKNOWLEDGMENT

The authors thank the support from the Foundation of Graduate Innovation Center in NUAA under Grant No. kfjj20170414, and the support from the Fundamental Research Funds for the Central Universities. National Natural Science Foundation of China (61501227, 61071019), Postdoctoral Science Foundation of China (2015M581789), 56YAH17032 of NUAA, Jiangsu Innovation Program for Graduate Education (KYLX16-0370), Fundamental Research Funds for the Central Universities (NJ20160011), MINECO-Spain (TEC2016-75650-R), Generalitat de Catalunya (2017SGR-1159) and FEDER funds. The authors also acknowledge the China Scholarship Council (CSC) for Grant 201706830064.

REFERENCES

1. Beth, R. A., "Mechanical detection and measurement of the angular momentum of light," *Physical Review*, Vol. 50, No. 2, 115–125, 1936.
2. Jackson, J. D., *Classical Electrodynamics*, Nuclear Physics, John Wiley & Sons Ltd., New York, 1963.
3. Allen, L., M. W. Beijersbergen, R. J. Spreeuw, and J. P. Woerdman, "Orbital angular momentum of light and the transformation of Laguerre-Gaussian laser modes," *Physical Review & Atomic Molecular & Optical Physics*, Vol. 45, No. 11, 81–85, 1992.
4. Gibson, G., et al., "Free-space information transfer using light beams carrying orbital angular momentum," *Optics Express*, Vol. 12, No. 22, 5448–5456, 2004.
5. Ren, Y., et al., "Experimental characterization of a 400 Gbit/s orbital angular momentum multiplexed free-space optical link over 120 m," *Optics Letters*, Vol. 41, No. 3, 622–625, 2016.
6. Yao, A. M. and M. J. Padgett, "Orbital angular momentum: Origins, behavior and applications," *Advances in Optics & Photonics*, Vol. 3, No. 2, 161–204, 2011.
7. Padgett, M. J. and L. Allen, "The angular momentum of light: Optical spanners and the rotational frequency shift," *Optical & Quantum Electronics*, Vol. 31, No. 1, 1–12, 1999.
8. Torner, L., J. Torres, and S. Carrasco, "Digital spiral imaging," *Optics Express*, Vol. 13, No. 3, 873–881, 2005.
9. Torres, J. P. and L. Torner, *Twisted Photons: Applications of Light with Orbital Angular Momentum*, Wiley-VCH, 2011.
10. Thidé, B., et al., "Utilization of photon orbital angular momentum in the low-frequency radio domain," *Physical Review Letters*, Vol. 99, No. 8, 087701, 2007.
11. Mohammadi, S. M., et al., "Orbital angular momentum in radio — A system study," *IEEE Transactions on Antennas & Propagation*, Vol. 58, No. 2, 565–572, 2010.

12. Tamburini, F., et al., "Encoding many channels in the same frequency through radio vorticity: First experimental test," *New Journal of Physics*, Vol. 14, No. 3, 811–815, 2011.
13. Lin, M., Y. Gao, P. Liu, and J. Liu, "Super-resolution orbital angular momentum based radar targets detection," *Electronics Letters*, Vol. 52, No. 13, 1168–1170, 2016.
14. Yuan, T., H. Wang, Y. Qin, and Y. Cheng, "Electromagnetic vortex imaging using uniform concentric circular arrays," *IEEE Antennas & Wireless Propagation Letters*, Vol. 15, 1024–1027, 2016.
15. Tamburini, F., et al., "Experimental demonstration of free-space information transfer using phase modulated orbital angular momentum radio," *Physics*, Vol. 13, No. 2, 20–25, 2013.
16. Zhang, Z., S. Zheng, X. Jin, H., Chi, and X. Zhang, "Generation of plane spiral OAM waves using traveling-wave circular slot antenna," *IEEE Antennas & Wireless Propagation Letters*, Vol. 16, 8–11, 2016.
17. Yu, S., L. Li, G. Shi, C. Zhu, X. Zhou, and Y. Shi, "Design, fabrication, and measurement of reflective metasurface for orbital angular momentum vortex wave in radio frequency domain," *Applied Physics Letters*, Vol. 108, No. 12, 5448, 2016.
18. Yu, S., G. Shi, C. Zhu, and Y. Shi, "Generating multiple orbital angular momentum vortex beams using a metasurface in radio frequency domain," *Appl. Phys. Lett.*, Vol. 108, No. 24, 241901, 2016.
19. Jin, J., et al., "Generation and detection of orbital angular momentum via metasurface," *Scientific Reports*, Vol. 6, 24286, 2016.
20. Chen, M. L. N., L. J. Jiang, and W. E. I. Sha, "Artificial perfect electric conductor-perfect magnetic conductor anisotropic metasurface for generating orbital angular momentum of microwave with nearly perfect conversion efficiency," *Journal of Applied Physics*, Vol. 119, No. 6, 064506, 2016.
21. Chen, M. L. N., L. J. Jiang, and W. E. I. Sha, "Ultrathin complementary metasurface for orbital angular momentum generation at microwave frequencies," *IEEE Transactions on Antennas & Propagation*, Vol. 65, No. 1, 396–400, 2017.
22. Chen, M., L. J. Jiang, and W. E. I. Sha, "Detection of orbital angular momentum with metasurface at microwave band," *IEEE Antennas & Wireless Propagation Letters*, Vol. 17, No. 1, 110–113, 2018.
23. Xu, H. X., H. Liu, X. Ling, Y. Sun, and F. Yuan, "Broadband vortex beam generation using multimode pancharatnam–berry metasurface," *IEEE Transactions on Antennas & Propagation*, Vol. 65, No. 12, 7378–7382, 2017.
24. Zhang, Y., L. Yang, H. Wang, X. Zhang, and X. Jin, "Transforming surface wave to propagating OAM vortex wave via flat dispersive metasurface in radio frequency," *IEEE Antennas & Wireless Propagation Letters*, Vol. 17, No. 1, 172–175, 2018.
25. Li, Y., B. Liang, Z. M. Gu, X. Y. Zou, and J. C. Cheng, "Reflected wave-front manipulation based on ultrathin planar acoustic metasurfaces," *Scientific Reports,* Vol. 3, 2546, 2013.
26. Yu, N., et al., "Light propagation with phase discontinuities reflection and refraction," *Science*, Vol. 334, 333–337, 2011.
27. Khorasaninejad, M., W. T. Chen, R. C. Devlin, J. Oh, A. Y. Zhu, and F. Capasso, "Metalenses at visible wavelengths: Diffraction-limited focusing and subwavelength resolution imaging," *Science*, Vol. 352, 1190–1194, 2016.
28. Ma, X., et al., "A planar chiral meta-surface for optical vortex generation and focusing," *Scientific Reports*, Vol. 5, 10365, 2015.
29. Holloway, C. L., E. F. Kuester, J. A. Gordon, J. O'Hara, J. Booth, and D. R. Smith, "An overview of the theory and applications of metasurfaces: The two-dimensional equivalents of metamaterials," *IEEE Antennas & Propagation Magazine*, Vol. 54, No. 2, 10–35, 2012.
30. Cai, B., L. Zhou, Q. He, S. Xiao, T. J. Cui, and X. Li, "Flat metasurfaces to focus electromagnetic waves in reflection geometry," *Optics Letters*, Vol. 37, No. 23, 4940–4942, 2012.
31. Fukumoto, H., H. Sasaki, D. Lee, and T. Nakagawa, "Beam divergence reduction using dielectric lens for orbital angular momentum wireless communications," *International Symposium on Antennas and Propagation IEEE*, 680–681, Okinawa, Japan, Oct. 2016.